# MANGO: Low-Cost Open Source Needle Guidance

J. V. Galvao da Mata[a], H. Krumb[b], U. Mishra[c], A. Mukhopadhyay[b], C. Essert[a]

[a]Université de Strasbourg, France; [b]Technische Universität Darmstadt, Germany; [c]Indian Institute of Technology, India

**ARTICLE HISTORY**
Compiled September 16, 2022

**ABSTRACT**
Validating experiments in intra-operative planning for percutaneous interventions requires to localize the needle with a tracking system. As commercial optical trackers are expensive, we present MANGO, a low-cost OpenSource solution for needle tracking. We first present the design of our system, which localizes colored orbs using a stereo-camera setup. Based on this setup, we investigate the static and dynamic error of the system, and experiment with signal filtering to improve tracking performance. With the MANGO, we are able to meet the positional accuracy margin of 5 mm usually required in percutaneous interventions. Orientational accuracy, measured by needle tip localization accuracy as a proxy measure, exceeds this margin. We plan to investigate this further in future research. Releasing our code, data and 3D models, we aim to provide a low-cost and reproducible platform for needle tracking and validation of intra-operative planning in research environments.

**KEYWORDS**
Navigation and Tracking; Optical Tracking; Needle Guidance

## 1. Introduction

Needle tracking is an essential tool to experimentally evaluate intra-operative planning methods for percutaneous interventions, such as biopsies in the abdomen, in laboratory settings. Thanks to its precision, optical tracking is a suitable technology for needle tracking in such phantom studies. However, although commercial solutions for optical needle tracking exist, those are often prohibitively expensive for small research labs. Further, commercial optical tracking systems require pre-calibrated infrared markers which are delicate in the handling and are relatively expensive themselves. While aiming at minimizing that cost, our goal is to create a tracking system suitable for needle biopsy which meets the accuracy requirements of such procedures. For instance, the accuracy margin of tumor ablation in liver is deemed to lie between 5 mm and 10 mm [4].

The high prices of commercial tracking systems motivated several works aiming at developing low cost tracking systems. For instance, Asselin et al. [1] used the information of a single webcam and a depth sensor to track markers attached to medical tools. However, their approach does not meet the required accuracy margin of 10 mm. Wang et al. [7] proposed to use the Microsoft Kinect to track needle-shaped objects. Although this low-cost approach met the required accuracy margin, the source code for needle tracking is not publicly available, which impedes reproducibility.

In this work, we introduce MANGO, a low-cost open source two-camera system

targeted at researchers and engineers working in the field of computer assisted surgery. The system itself is comprised of two low-cost USB webcams that are rigidly aligned inside a 3D printed enclosure. With this setup, it is possible to track colored orbs that can be attached to surgical instruments and needles.

First, we outline the design of our system, as well as the software we used to track the colored markers. We then explore the limitations of our custom system and investigate filtering techniques and spatial constraints to improve the tracking accuracy. Using a commercial tracking system for the purpose of validation, we finally verify that our system meets the required accuracy margin.

## 2. Methods

The MANGO system is composed of a specific system made of two webcams in a 3D printed case and some colored orbs attached to the needle, as well as a software pipeline to calibrate the cameras, track the 3D markers, and estimate the pose of the needle and the position of its tip. The design of the system and the pipeline are described below.

### *2.1. System Design*

The hardware setup of the MANGO system consists of two webcams and a 3D printed case which protects the two cameras and constrains them not to move in relation to each other, as can be seen in Fig. 1 left. Several camera models were tested. In the most advanced models, which are often the most expensive, the autofocus results in a variable camera matrix, that makes it inappropriate for this project where a fixed matrix is required to avoid recalibration. On the other hand, the simplest (and cheapest) cameras usually have a lot of radial distortion resulting in large errors. The Logitech C270 HD camera was chosen because it combines low cost (under 30 USD/EUR per camera at the time of this experiment) with low levels of radial distortion and no autofocus feature.

Finally, the system is completed by four plastic orbs of different colors fixed on a holder attached to the needle, as illustrated on Fig. 1 right. For the experiment, the MANGO orbs were placed on one side of the holder, while NDI Polaris infrared reflective orbs were placed symmetrically on the reverse side of the holder.

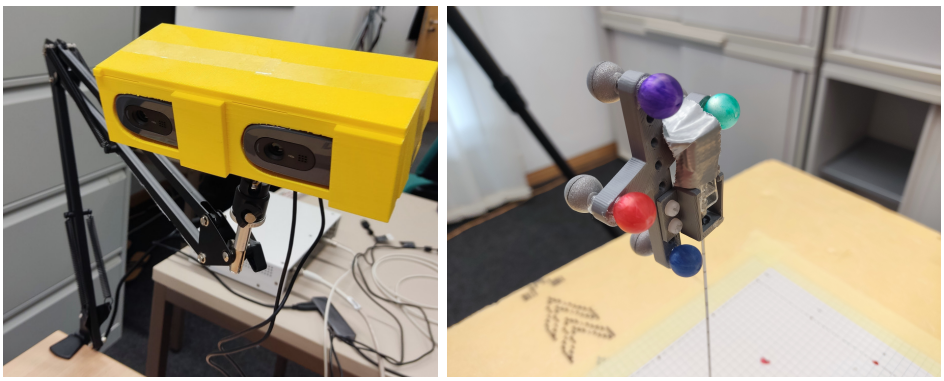

**Figure 1.** Left: The MANGO stereo-camera tracking system mounted on an adjustable arm. Right: Needle and 3D printed holder with infrared-reflective (Polaris) and colored (MANGO) orbs.

### *2.2. Calibration*

The two cameras are calibrated using a Direct Linear Transformation (DLT)-like method as proposed by Zhang [8]. This method uses several images of a planar object (in this work a chessboard pattern is used, as seen in Fig. 2) and returns the camera matrix with the intrinsic parameters and the transformation between the camera frame and the object frame for each picture. The average reprojection error found for all the points was 0.01533 pixels for the right camera and 0.01461 pixels for the left camera.

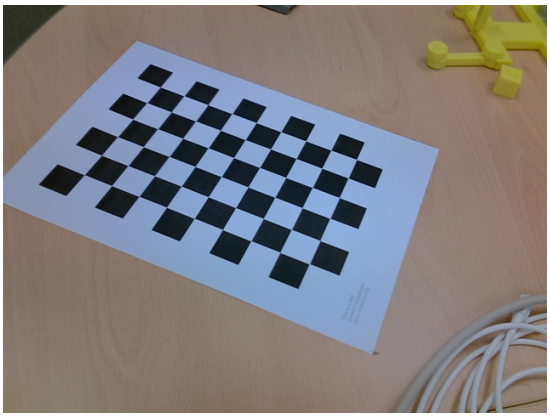

**Figure 2.** One of the chessboard patterns used in the calibration.

For each pair of images, the transformation between the two camera frames is computed from the transformations between each camera frame and the chessboard frame. Then the final transformation is given by the average translation vector and the rotation matrix generated by the average Euler angles for all the transformations for each pair of images.

### *2.3. Orb Tracking*

A color-based tracking strategy is used to localize the colored orbs, compute the position and orientation of the needle and its tip. For each image, the first step is to convert the color space from the traditional RGB to the HSV color space, where it is easier to segment colors just defining a hue range, and then refining the segmentation using the saturation and value. With that segmentation, a mask is created and used as basis for a contour detection algorithm [6]. The center of mass of this contour is then recovered as an estimate for the orb center. This process is illustrated in Fig. 3.

In order to estimate the 3D pose of the needle, at least three non-aligned orbs need to be detected successfully. A fourth orb is attached to the marker as a backup in case another orb is not visible, e.g. due to reflections or occlusion. Each orb has its own color, which allows their individual tracking independently, as shown in Fig. 4.

The 3D position of each orb can be then deduced from their center position on the image of both cameras, the transformations between the cameras, and the camera matrices, using triangulation.

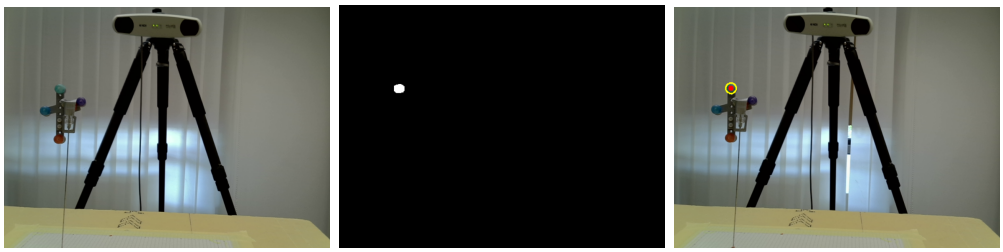

**Figure 3.** (Left) Double-sided marker as seen by the stereo camera system. (Center) Mask of the green orb which is used for tracking (Right). The Polaris system in the background is used for validation.

**Figure 4.** (Left) 4 orbs. (Right) Tracking result.

### *2.4. Estimation of the Coordinate Frame and Needle Tip Tracking*

The shape of the multi-orb marker was chosen to allow recovery of all six degrees of freedom of the instrument and provide some redundancy.

Using a single orb, only the three positional coordinates of the orb can be recovered. With two orbs, a direction vector can also be found. With three or more orbs the entire six Degrees of Freedom (DOF) of the instrument can be detected, i.e. both the three coordinates and the orientation of the needle can be tracked, so that the position of the tip can be found.

A coordinate frame for the marker is defined as shown in Fig. 5. Knowing the position of the center of each orb in this coordinate frame and the coordinate frame of the camera, the transformation between both frames can be found. Then as the needle tip position is known in relation to the marker frame, it can be described in the camera coordinate frame.

## 3. Validation Protocol

We assessed the tracking accuracy of the MANGO system by comparing the tracking results with an NDI Polaris Vicra system. The Polaris Vicra has a stated accuracy of 0.5 mm (CI-95), and thus serves as a proper reference standard we can use for our experiments. The needle and attached marker set was partly inserted and fixed into a rigid foam structure to reduce oscillations due to movements, as shown in Fig. 6 (right). This setup was manually moved so that the needle tip sequentially covered a grid of points evenly spaced by 2 cm × 2 cm. The positions of the orbs were measured with both MANGO and Polaris systems simultaneously and continuously recorded. At each point of the grid, we let the needle and markers stabilize for 20 s. The recorded data points

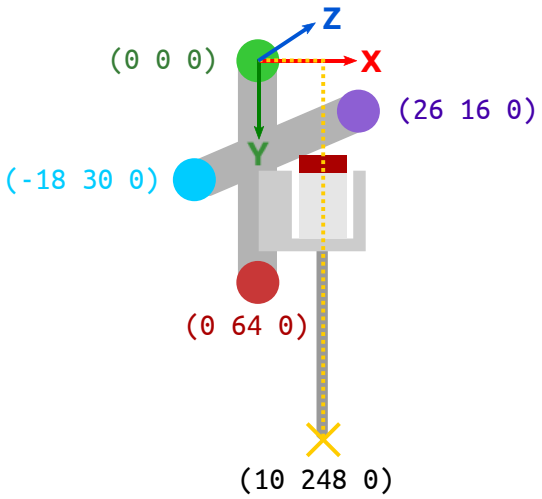


**Figure 5.** Marker geometry and coordinate frame.

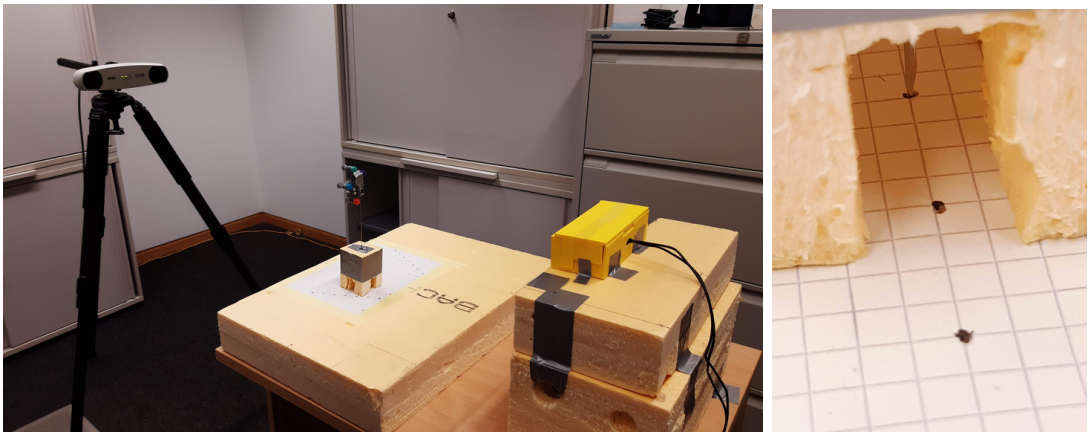

**Figure 6.** Left: Comparing the MANGO to the NDI Polaris with a two-faced marker fixture. Right: The needle is positioned precisely with the styrofoam fixture.

were first aligned to a common coordinate frame by using Horn's method [5] under the use of eight extra calibration points that were collected with a similar protocol.

The time vector for both system was collect using the UNIX timestamp. As the MANGO sample rate is 30 Frames per Second (FPS) and the Polaris NDI sample rate is 50 FPS, the reference time vector used was that of MANGO. For each data point of the MANGO the comparison was done with the closest corresponding timestamp of the NDI Polaris.

In a second step, we estimated the series of positions of the needle tip for both tracking devices to properly compare the systems in six DOF. A sequence of stabilized positions was computed for the marker and the needle tip by clustering the time series of positions. DBSCAN was used for this clustering [3] ($\epsilon = 1.5\,\text{mm}$, 200 samples), as it is well-established and separates noisy samples outside the cluster centers (we used these outliers to calculate the dynamic error in Sec. 4.3). Unlike traditional k-means, DBSCAN does not require the number of cluster centers to be known beforehand. Rather, DBSCAN separates data points based on the cluster density, such that the distribution of cluster points would not need to be spherical. The density parameter

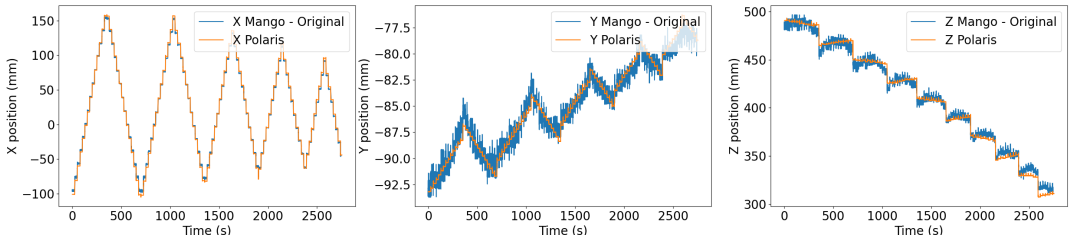


**Figure 7.** Comparison between the raw data of MANGO (blue) and the data collected with the Polaris System (orange).The three figures correspond respectively to the x, y and z coordinates measured by both systems.

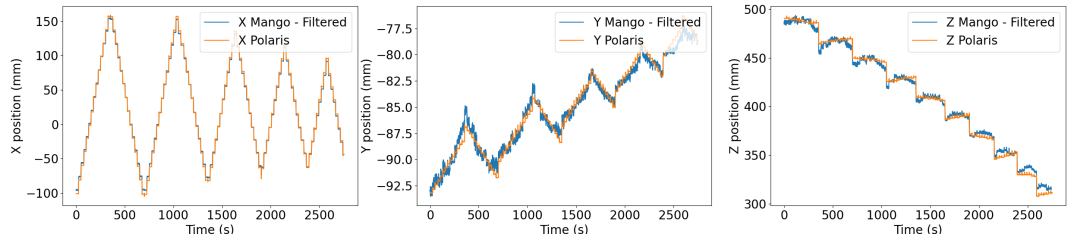


**Figure 8.** Comparison between the filtered data of MANGO and the data collected with the Polaris System.

$\epsilon$ was gauged between twice the stated accuracy of the Polaris (1 mm) and half the distance between measuring points (10 mm), to allow for slight deviations of measurements from the stated tracking accuracy still being considered *static* measurements when analyzing static vs. dynamic accuracy.

All experimental code was written in Python with the use of OpenCV framework [2].

## 4. Experimental Results

In this section, we present the experimental results we obtained by following the measurement protocol described in Sec. 3. Fig. 7 shows the comparison between the positions in x, y, and z obtained with the Polaris system and the MANGO system without any filtering strategy applied.

### *4.1. Filtering Strategies*

Variations in the amount of light in the room, movements in the background, and the cameras' auto-exposure feature affected the color tracking strategy and caused oscillations in detecting the center of each orb in the images as can be seen in Fig. 7, especially in z direction. A Gaussian filter was applied with a window size of 15 samples (0.5 seconds). This size was chosen to attenuate the oscillations due the color without attenuating the natural oscillations of the needle. The new results after the filtering can be seen in Fig. 8.

The first two rows of Tab. 1 show the Root Mean Squared Error (RMSE) and Mean Absolute Error (MAE) of the x, y and z coordinates for filtered and unfiltered data respectively. The filtering slightly improved the error in the y and z directions.

| | $RMSE_X$ [mm] | $RMSE_Y$ [mm] | $RMSE_Z$ [mm] | $MAE_X$ [mm] | $MAE_Y$ [mm] | $MAE_Z$ [mm] |
|---|---|---|---|---|---|---|
| Full volume, no filter | 2.75 | 0.68 | 4.49 | 2.27 | 0.55 | 3.62 |
| Full volume, Gaussian filter | 2.75 | 0.64 | 4.39 | 2.27 | 0.52 | 3.53 |
| Optimal volume, G. filter | 1.29 | 0.43 | 1.89 | 0.99 | 0.37 | 1.60 |
| Decrease of error | 53.1% | 32.8% | 56.4% | 56.4% | 28.8% | 54.7% |

**Table 1.** Comparison of the Root Mean Squared Error (RMSE) and Mean Absolute Error (MAE) of the x, y and z coordinates for filtered and unfiltered data, optimal tracking volume (with filter applied). All values are denoted in mm.

| | $RMSE_X$ [mm] | $RMSE_Y$ [mm] | $RMSE_Z$ [mm] | $MAE_X$ [mm] | $MAE_Y$ [mm] | $MAE_Z$ [mm] |
|---|---|---|---|---|---|---|
| Static, full volume | 2.72 | 0.68 | 4.47 | 2.25 | 0.55 | 3.60 |
| Static, optimal volume | 1.14 | 0.49 | 2.06 | 0.87 | 0.41 | 1.72 |
| Dynamic, full volume | 3.29 | 0.81 | 4.84 | 2.62 | 0.63 | 3.98 |
| Dynamic, optimal volume | 2.38 | 0.66 | 2.91 | 1.94 | 0.55 | 2.51 |

**Table 2.** Comparison of the Root Mean Squared Error (RMSE) and Mean Absolute Error (MAE) of the x, y and z coordinates static vs. dynamic error (with filter) in both full and optimal volume. All values are denoted in mm.

### *4.2. Optimal Tracking Volume*

Looking at Fig. 8, it can be noted that the error increased when the needle approached the sides or the front of the working space. This effect is probably due to the radial distortion of the lens. Using a color scale, Fig. 9 shows the the error for each measured position in the x-z plane, as well as the optimal area where the smallest errors can be found (represented as a red trapezoid).

As can be seen in Tab. 1 (rows 3 and 4) errors inside the optimal volume were half of the error in the overall area in the x and z directions, and around two thirds in the y direction.

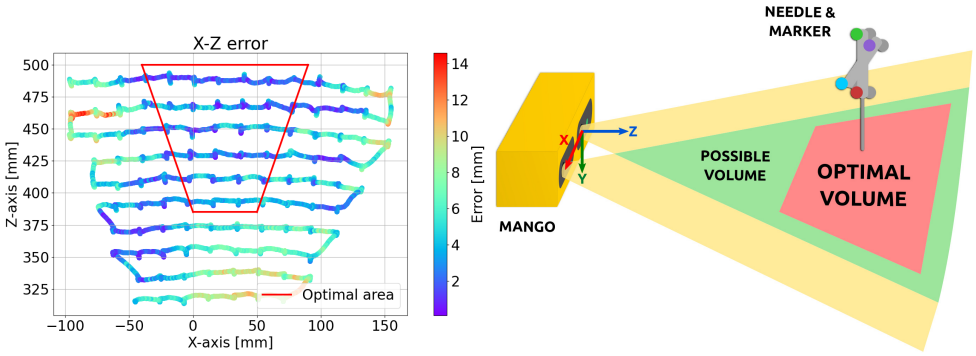


**Figure 9.** Left: Positional error of the MANGO in its X - Z plane, the red trapezoid highlights the optimal tracking volume. Right: Illustration of possible and optimal tracking space.

### *4.3. Static vs. Dynamic Error*

To assess the dynamic and static error of the MANGO, we separated the stabilized points obtained with the DBSCAN clustering from the outliers, the latter corresponding to the needle movements in between the points. For each corresponding timestamp

of the two datasets (Polaris and MANGO), we compared the corresponding points for (a) static inliers and (b) dynamic outliers to calculate an error estimate. The static and dynamic errors are reported in Tab. 2 for both the full and the optimal tracking volumes.

We can see that the MANGO also meets the accuracy requirements if the needle is in motion, as the dynamic tracking error is only slightly higher but still below the 5 mm margin. The dynamic accuracy is sufficient in the *full* tracking volume, but is significantly better when confined to the optimal tracking space.

### *4.4. Needle Tip Tracking Error*

Until now we only evaluated the tracking of three DOF of the marker, i.e. the tracking of the orb at the origin of the marker coordinate frame (or the translation vector between the marker frame and the camera frame). In this section we evaluate the tracking of the needle tip, which requires all six DOF, and allows to indirectly assess the measured orientation of our marker.

Fig. 10 shows the comparison between the tracking of the needle tip with MANGO and with the Polaris System inside the optimal volume. Tab. 3 shows the errors for the three coordinates. The Polaris system itself provides measurement data for all six degrees of freedom out-of-the-box.

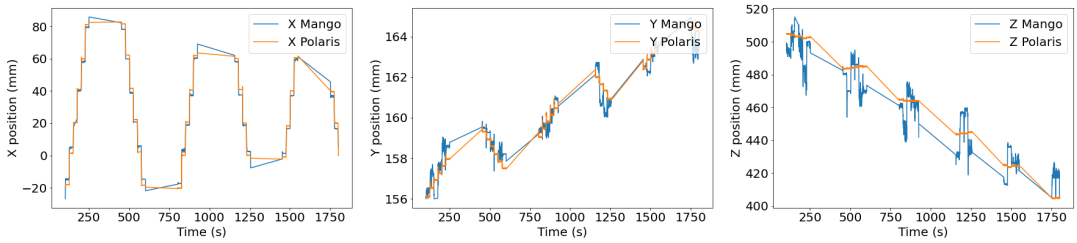


**Figure 10.** Comparison between the tracking of the needle tip with MANGO and with the Polaris System inside the optimal volume.

| $RMSE_X$ | $RMSE_Y$ | $RMSE_Z$ | $MAE_X$ | $MAE_Y$ | $MAE_Z$ |
|---|---|---|---|---|---|
| 2.62 | 0.58 | 11.48 | 2.38 | 0.45 | 9.29 |

**Table 3.** Comparison of the Root Mean Squared Error and Mean Absolute Error of the x, y and z coordinates for the needle tip inside the optimal volume. All values are denoted in mm.

While the error is below the accuracy margin of 5mm [4] requested for our intended use case in the x and y directions, it can be observed that the error in the z coordinate is around ten millimeters, which exceeds the margin. As the main cause of this error, we identified the oscillations in the color tracking of each orb due to slight variations of light, that remained too high even with the Gaussian filter. Indeed, due to the length of the needle, a slight inaccuracy in the tracking of the marker set has a high influence on the accuracy of the tracking of the needle tip, specially in the depth direction.

Three main solutions can be investigated in a future study in order to reduce the error in the tracking of the needle tip, such as considering tracking approaches that would not rely on color or less sensitive to light variations, working in a controlled environment without light variations, using orbs with a different material or trying active markers such as LEDs, improving the filtering, or trying different marker geometries.

## 5. Conclusion

In this paper, we have presented MANGO, a low-cost open source optical tracking system for needle navigation intended to be used in lab studies for needle tracking in percutaneous intervention guidance. Based on a stereo-camera system and colored orbs, markers attached to a biopsy needle are tracked in six DOF thanks to a color-based approach. Using a commercial tracker as a reference system, we observed that MANGO met the positional accuracy requirements in terms of 3D position of the marker set. Using the estimation of the needle tip position as a proxy for orientation, we found that the detection of the orientation in the plan perpendicular to the cameras (x and y directions) also met the expected accuracy. However, one current limitation of our system is that tracking the orientation in the z direction (depth of the needle tip) was negatively affected by slight variations of light that caused oscillations in the individual orb detection. In the future, we plan to address this issue by investigating alternative tracking techniques, environments, or markers. We further aim to explore the potential of cascading multiple MANGOs to increase the tracking volume and accuracy, as illustrated in Fig. 11.

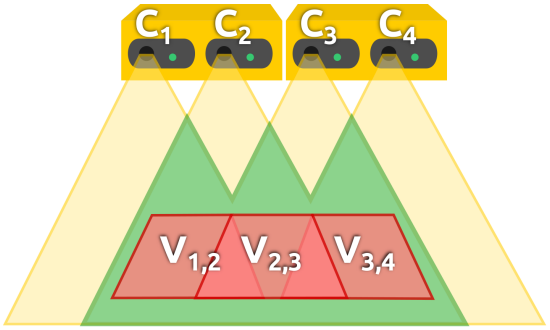


**Figure 11.** Cascading multiple MANGO systems potentially increases the maximum optimal tracking volume (red). Positioning two MANGOs side-by-side, the two cameras $C_2$ and $C_3$ with intersecting fields-of-view can be leveraged to generate a continuous optimal volume in the shape of a wide trapezoid.

With a total price of only 60 USD/EUR, our proposed system is by far cheaper than commercial systems, which may cost up to several thousands of USD/EUR. By making all our code, 3D models and experimental data public[1] under a free license, we aim to facilitate the reproduction of the system in other research labs to accelerate research in the field of pre-operative planning and needle guidance for percutaneous interventions.

## Acknowledgements

This work of the Interdisciplinary Thematic Institute HealthTech, as part of the ITI 2021-2028 program of the University of Strasbourg, CNRS and Inserm, was supported by IdEx Unistra (ANR-10-IDEX-0002) and SFRI (STRAT'US project, ANR-20-SFRI-0012) under the framework of the French Investments for the Future Program.

[1]Code, data and models: `https://github.com/Jvictormata/mango`

## References


[1] Asselin M, Ungi T, Lasso A, Fichtinger G. 2018. A training tool for ultrasound-guided central line insertion with webcam-based position tracking. In: Simulation, Image Processing, and Ultrasound Systems for Assisted Diagnosis and Navigation - Proceedings of MICCAI workshops POCUS 2018, BIVPCS 2018, CuRIOUS 2018, CPM 2018; (LNCS; vol. 11042). Springer International Publishing. p. 12–20.

[2] Bradski G. 2000. The OpenCV Library. Dr Dobb's Journal of Software Tools.

[3] Ester M, Kriegel HP, Sander J, Xu X. 1996. A density-based algorithm for discovering clusters in large spatial databases with noise. In: Proceedings of the Second International Conference on Knowledge Discovery and Data Mining. AAAI Press. p. 226–231. KDD'96.

[4] Goldberg SN, Grassi CJ, Cardella JF, Charboneau JW, Dodd III GD, Dupuy DE, Gervais D, Gillams AR, Kane RA, Lee Jr FT, et al. 2005. Image-guided tumor ablation: Standardization of terminology and reporting criteria. Journal of Vascular and Interventional Radiology. 16(6):765–778.

[5] Horn BK, Hilden HM, Negahdaripour S. 1988. Closed-form solution of absolute orientation using orthonormal matrices. Journal of the Optical Society of America A (JOSA A). 5(7):1127–1135.

[6] Suzuki S, Abe K. 1985. Topological structural analysis of digitized binary images by border following. Comput Vis Graph Image Process. 30:32–46.

[7] Wang XL, Stolka PJ, Boctor E, Hager G, Choti M. 2012. The Kinect as an interventional tracking system. In: III DRH, Wong KH, editors. Medical Imaging 2012: Image-Guided Procedures, Robotic Interventions, and Modeling; vol. 8316. International Society for Optics and Photonics; SPIE. p. 276 – 281.

[8] Zhang Z. 2000. A flexible new technique for camera calibration. IEEE Transactions on pattern analysis and machine intelligence. 22(11):1330–1334.